Dynamic Modeling and Closed-loop Control of Hybrid Grid-connected Renewable Energy System with Multi-input Multi-output Controller

Mahdi Salimi, Fereshteh Radmand, and Mansour Hosseini Firouz

***Abstract*—In this study, a novel approach for dynamic modeling and closed-loop control of hybrid grid-connected renewable energy system with multi-input multi-output (MIMO) controller is proposed. The studied converter includes two parallel DC-DC boost converters, which are connected into the power grid through a single-phase H-bridge inverter. The proposed MIMO controller is developed for maximum power point tracking of photovoltaic (PV)/fuel-cell (FC) input power sources and output power control of the grid-connected DC-AC inverter. Considering circuit topology of the system, a unique MIMO model is proposed for the analysis of the entire system. A unique model of the system includes all of the circuit state variables in DC-DC and DC-AC converters. In fact, from the viewpoint of closed-loop controller design, the hybrid grid-connected energy system is an MIMO system. The control inputs of the system are duty cycles of the DC-DC boost converters and the amplitude modulation index of DC-AC inverters. Furthermore, the control outputs are the output power of the PV/FC input power sources as well as AC power injected into the power grid. After the development of the unique model for the entire system, a decoupling network is introduced for system input-output linearization due to inherent connection of the control outputs with all of the system inputs. Considering the decoupled model and small signal linearization, the required linear controllers are designed to adjust the outputs. Finally, to evaluate the accuracy and effectiveness of the designed controllers, the PV/FC based grid-connected system is simulated using the MATLAB/Simulink toolbox.**

***Index Terms*—Multi-input multi-output (MIMO) converter, maximum power point tracking, grid-connected inverter, conversion function matrix.**

I. Introduction

GRID-CONNECTED voltage source inverters have been widely used in active power filters, online uninterruptable power supplies, and renewable energy systems [1]. In these applications, output power control and DC-link voltage regulation should be performed. Related to the importance of greenhouse gas reduction, renewable energy sources such as photovoltaic (PV) systems, fuel cells (FCs), and wind turbines have been extensively employed to respond to the increasing electrical energy demand. Additionally, the application of the PV energy has gained considerable attention in recent years due to the widespread global existence of solar energy. Moreover, with recent developments in solar energy technology, the capital cost of PV systems has been sharply reduced [2]. It should be noted that the applications of grid-connected PV systems are preferred due to the removal of storage batteries. In such applications, usually DC-DC and DC-AC converters are required for the maximum power point tracking (MPPT) of the renewable power source and the conversion of the PV output into AC power, respectively. From the viewpoint of controller design, the closed-loop control of the grid-connected systems is a challenging task due to the cascade connection of multiple converters.

Considering a multiport DC-DC converter, a PV panel and a backup battery are connected to the DC link of a single-phase grid-connected inverter in [3]. Linear controllers are employed for the MPPT of the PV generator and the regulation of the system output power. However, the controllers are not designed using a dynamic model of the system, and the gains of compensators are selected by trial and error.

In [4], a bidirectional single-stage grid-connected inverter is studied for energy storage systems. Several buck-boost DC-DC choppers have been employed for the connection of the batteries into the system DC link. Considering the steady-state behavior of the system, some equations are obtained for power flow control of the storage batteries. The controlling system does not require any current sensors. As the controller is developed based on steady-state analysis, it cannot guarantee system stability in different operation conditions.

Considering the mathematical model of the multi-parallel inverters, intrinsic and extrinsic resonances are studied in microgrid applications [5]. Moreover, to attenuate the resonance of the system, an active damping control approach is developed. In [5], the PV module and DC-DC converter are modeled as a constant DC voltage source. However, it is well known that in grid-connected inverters, the DC link has considerable voltage ripple. Moreover, the developed controller is unable to track the maximum power point (MPP) of the input power source.

Manuscript received: June 17, 2018; accepted: January 23, 2020. Date of CrossCheck: January 23, 2020. Date of online publication: January 11, 2021.

This work was supported by Islamic Azad University – Ardabil Branch.

M. Salimi (corresponding author), F. Radmand, and M. H. Firouz are with the Department of Electrical Engineering, Ardabil Branch, Islamic Azad University, Ardabil, Iran (e-mail: m.salimi@iauardabil.ac.ir; f.radmand@iauardabil.ac.ir; hosseini.firooz@iauardabil.ac.ir).

DOI: 10.35833/MPCE.2018.000353

In grid-connected PV systems, an attempt is made to maximize the total circuit efficiency by minimizing the number of required converters. For example, in [6]-[8], an attempt is made to improve the power efficiency of the grid-connected PV systems by removing DC-DC converters. In this condition, the MPPT of the input power source is accomplished by DC-side voltage control of the inverter. However, in [6]-[8], series connection of multiple solar panels is necessary to increase DC-link voltage in the transformerless grid-connected PV systems. The primary disadvantage of the panels' series connection appears during partial shading. Due to the current reduction in the shaded cells, the total output power will decrease considerably in series-connected PV panels. Conversely, the application of 50 Hz bulky transformers in the inverter output for the grid connection of the PV systems is undesirable due to its high weight and cost. Briefly, a voltage boost of the PV output power is required in grid-connected systems by using a step-up DC-DC converter [9]-[11].

Low-frequency power mitigation control is studied for grid-connected PV systems by using a dynamic model based controller [12]. Considering low-voltage ripple of the DC link, small capacitors can be used in the grid-connected inverter. In addition, the MPPT of input PV sources can be performed with fast tracking speed. However, a developed controller cannot be employed in hybrid renewable energy systems. Due to the dependence of the generated PV power on radiance level, temperature, and shading conditions, and the lack of power generation during night hours, PV systems are normally combined with other energy sources or storage systems to improve the reliability of the renewable power plant. If the hybrid renewable energy system is equipped with an appropriate controller, it can demonstrate better reliability for load power supply [13] compared with a single-source system. FC generator is an ideal option for combination with PV systems [14] due to acceptable power efficiency and independence from weather conditions.

Recently, the research and development of the hybrid renewable energy system have increased. For example, in [15], a backstepping nonlinear controller is designed for hybrid PV power supplies for remote communication applications. To supply system loads, a buck/boost DC-DC converter is cascaded with a single-phase DC-AC inverter. A nonlinear backstepping controller guarantees the stability and robustness of the designed controllers during system parameter changes. However, in [15], the DC-DC converter and DC-AC inverter are modeled as separate subsystems. Hence, inherent connections between these subsystems are not considered. In fact, the multi-input multi-output (MIMO) model of the cascaded converters is not used for controller design. Moreover, the practical implementation of the backstepping controller [16] requires very fast processors and digital/analog (D/A) converters. Furthermore, gains of the controllers in [15] are selected by trial and error.

The analysis of a grid-connected PV-wind-battery hybrid energy system is presented in [17], [18], which includes energy engineering concepts, reliability, and cost reduction studies of the plant. However, dynamic analysis and system modeling are not studied in [17], [18].

In [19], a novel three-input DC-DC converter for stand-alone PV-FC battery systems is proposed. The MPPT of the PV panel and FC system is studied. The linear controllers are designed based on small signal analysis of the model. However, the controller of [19] is only applicable to stand-alone renewable systems and dynamic modeling of the DC-AC inverter which is employed in the grid-connected system is not reported. It is clear that adding the AC-side state variables into the converter model complicates the development of the unique general model for the entire system, and also increases the difficulty of the controller design.

In [20], the closed-loop control of the grid-connected inverters is studied to improve the current quality and active power filtering in the distribution system. In spite of the non-ideal waveform of the grid voltage, the developed controller is able to compensate nonlinear and harmonic components of the local load. Furthermore, it is not required to transfer coordinates of system voltages and currents. Hence, the control law can be calculated simply, which results in ease of practical implementation.

In [21], the nonlinear robust control of PV systems is studied. The proposed controller is designed to track the MPP of the input power source, regulate DC voltage of the inverter, as well as active power injected into the power grid. To protect the system from inverter faults during voltage dips, a reactive power injection capability is provided for the system. It can be used during normal grid-connected conditions as well as stand-alone fault mode. Two separate models at AC inverter side and DC chopper side are employed for nonlinear control of the system.

Utility fault ride-through capability of the grid-connected renewable energy systems is investigated in [22] using predictive controllers. In addition to standard capabilities of the grid-connected PV system, the controller can provide reactive power for load compensation and unity power factor operation. During voltage dips, the controller stops active power injection and the system operates as an active power filter.

In [23], the circuit topology of current source grid-connected inverters is modified to improve system response during voltage spikes of the grid voltage. It is realized by adding a standard buck chopper between input renewable power source and a current source inverter. Hence, in this structure, the PV panel current pulsates resulting in the oscillation of the operation point.

Briefly, in grid-connected renewable systems, a DC-DC converter can be cascaded with a DC-AC inverter for the grid connection of the input power source. In this structure, a DC-DC converter is employed for MPPT of the renewable power source. Additionally, a DC-AC inverter is responsible for AC power flow control between the renewable generator and the utility. To simplify the controller design, the input power source and the DC-DC chopper can be approximated as a constant DC voltage source [12]. In this condition, the modulation index (control input) of the grid-connected invert-

er is employed for AC current (control output) control. Hence, the renewable energy system can be approximated as a single-input single-output (SISO) system.

However, the DC link of the grid-connected inverter may include considerable voltage ripples. Hence, it cannot be approximated by a simple constant voltage source in a wide range of operation. In brief, to provide more accurate system control, the cascaded DC-DC and DC-AC converters must be considered as a unique system in grid-connected renewable energy systems. In this condition, the duty cycle of the chopper should be considered for the MPPT of the input power source. Furthermore, the modulation index of the inverter is employed for output power control. In fact, if a unique model is employed for controller design, the grid-connected system will include two different control inputs (including the duty cycle of the chopper and the modulation index of the inverter) and two different control outputs (including the input power of the renewable energy source and the grid current). Hence, the mentioned renewable generator is a MIMO system [24]. In spite of the superior response of the MIMO design, considering inherent connection among control inputs and outputs, it is clear that the MIMO controller design is significantly challenging compared with SISO systems.

In this study, the modeling and control of the grid-connected PV/FC hybrid energy systems are studied. The circuit topology consists of two separate DC-DC boost converters for the MPPT of the input sources. These choppers supply the DC link of the grid-connected inverter. In the proposed approach, a complete unique MIMO model of the system is employed for controller design. The control inputs of the system are duty cycles of the DC-DC boost converters and the amplitude modulation index of the DC-AC inverter. In addition, the system control outputs are the power from the PV/FC sources and the AC power injected into the power grid. Hence, from the viewpoint of controller design, the studied system is a three-input three-output circuit. Considering the complexities of controller design due to inherent connection between control outputs and all of the system inputs, a special decoupling network is employed to decouple controlling loops. Finally, considering small signal linearization of the MIMO model, system controllers are designed according to Bode analysis. Briefly, the primary contributions of this study can be summarized as follows:

1) Develope a general unique model for the MIMO hybrid energy system.

2) Develope a decoupling network and systematic design of the linear controllers for decoupled loops using Bode analysis.

The rest of this paper is organized as follows. The converter structure and its analysis are explained in Section II. Then, dynamic modeling of the converter is introduced in Section III. In Section IV, controller design and decoupling networks are presented. Finally, the simulation results of the controller are illustrated in Section V.

II. Converter Topology and Modeling

The topology of the MIMO converter, which will be considered in this study, is shown in Fig. 1. According to bipolar pulse width modulation of the inverter [25], it can be concluded that the inverter output voltage is ux_3. Moreover, its input current will be equal to ux_4. u, x_3, and x_4 are the amplitude modulation index, inverter DC-link voltage, and grid current, respectively. Considering these assumptions, the equivalent circuit of the system is shown in Fig. 2. The proposed converter has two input sources v_1 (PV) and v_2 (FC). The DC-DC converters are employed for the MPPT of the input power sources. Duty cycles of the switches S_1 and S_2 (d_1 and d_2) are control inputs of the DC-DC boost converters. Additionally, u is the control input of the DC-AC grid-connected inverter in the hybrid energy system. Equivalent circuits of the MIMO converter in different operation modes are shown in Fig. 3, where T is the switching period of DC-DC boost converters. Moreover, the steady-state waveforms of the DC-DC boost converters are illustrated in Fig. 4, where X_{G1} and X_{G2} are the gate signals of the S_1 and S_2, respectively.

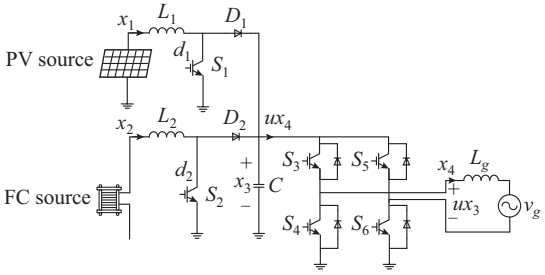

Fig. 1. Grid-connected PV/FC hybrid energy system.

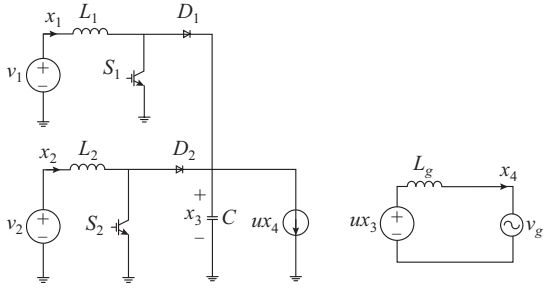

Fig. 2. Equivalent circuit of grid-connected PV/FC hybrid energy system.

According to Fig. 4, three different operation modes can be considered as $0 < t < d_1T$, $d_1T < t < d_2T$, and $d_2T < t < T$ intervals. By choosing the system state vector as $\boldsymbol{X}^{\mathrm{T}} = [i_{L_1}, i_{L_2}, v_C, i_{L_g}] = [x_1, x_2, x_3, x_4]$, an averaged state-space model of the system can be extracted, where v_C is the output capacitor voltage; i_{L_1} is the PV current; i_{L_2} is the FC current; and i_{L_g} is the grid current. During the first operation mode for $0 < t < d_1T$, it is observed that switches S_1 and S_2 are on. Hence, inductors L_1 and L_2 are charged through input voltage sources v_1 and v_2, respectively. Considering Fig. 3(a), state-space equations of the related sub-circuit can be written as follows:

$$\dot{\boldsymbol{X}} = \boldsymbol{A}_1 \boldsymbol{X} + \boldsymbol{B}_1 \tag{1}$$

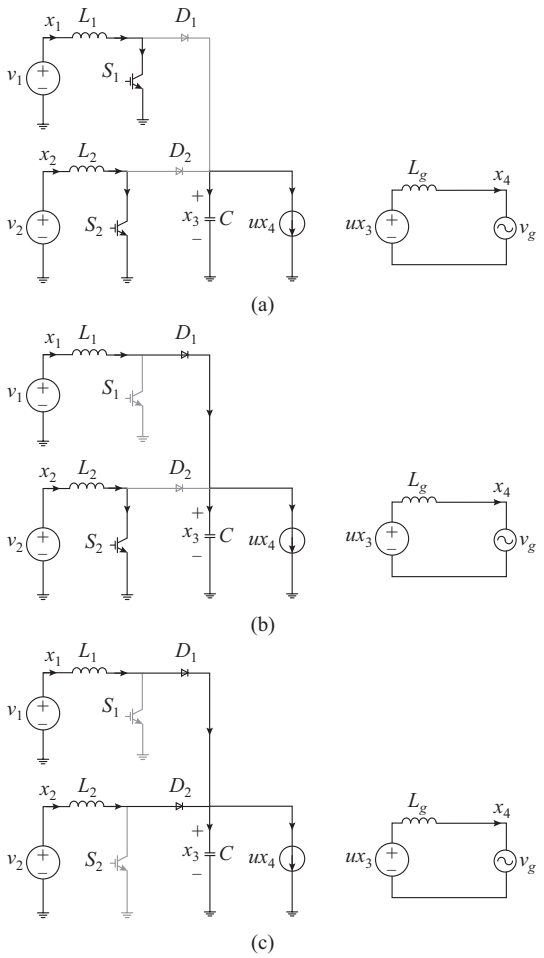

Fig. 3. Equivalent sub-circuits of converter in different operation modes. (a) The first kind of equivalent sub-circuit during $0<t<d_1T$. (b) The second kind of equivalent sub-circuit during $d_1T<t<d_2T$. (c) The third kind of equivalent sub-circuit during $d_2T<t<T$.

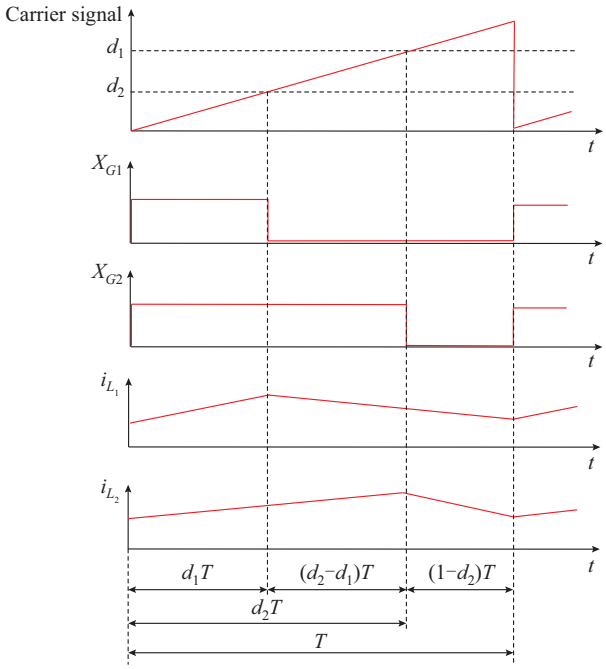

Fig. 4. Steady-state waveforms of DC-DC boost converters in grid-connected PV/FC hybrid energy system.

$$\begin{cases} \boldsymbol{A}_1 = \begin{bmatrix} 0 & 0 & 0 & 0 \\ 0 & 0 & 0 & 0 \\ 0 & 0 & 0 & -u/C \\ 0 & 0 & 0 & 0 \end{bmatrix} \\ \boldsymbol{B}_1 = \begin{bmatrix} V_1/L_1 & 0 & 0 & 0 \\ 0 & V_2/L_2 & 0 & 0 \\ 0 & 0 & 0 & 0 \\ 0 & 0 & 0 & -V_g/L_g \end{bmatrix} \end{cases} \tag{2}$$

where C is the DC-link capacitor of the inverter; V_1 and V_2 are the voltages of PV and FC sources, respectively; V_g is the grid voltage; and L_g is the coupling inductor.

According to Fig. 3(b), if it is assumed that $d_1<d_2$, it can be concluded that S_1 will be turned off at $t=d_1T$ during the second operation interval. However, S_2 is still conducting. Hence, the voltage of L_1 will be equal to v_1-v_C. Similarly, the following equations can be written during the second switching interval:

$$\dot{\boldsymbol{X}} = \boldsymbol{A}_2\boldsymbol{X} + \boldsymbol{B}_2 \tag{3}$$

$$\begin{cases} \boldsymbol{A}_2 = \begin{bmatrix} 0 & 0 & -1/L_1 & 0 \\ 0 & 0 & 0 & 0 \\ 1/C & 0 & 0 & -u/C \\ 0 & 0 & u/L_g & 0 \end{bmatrix} \\ \boldsymbol{B}_2 = \begin{bmatrix} V_1/L_1 & 0 & 0 & 0 \\ 0 & V_2/L_2 & 0 & 0 \\ 0 & 0 & 0 & 0 \\ 0 & 0 & 0 & -V_g/L_g \end{bmatrix} \end{cases} \tag{4}$$

Finally, in the third switching interval ($d_2T<t<T$), it is observed that both of the switches S_1 and S_2 are off and the state equations of the sub-circuit can be obtained according to Fig. 3(c).

$$\dot{\boldsymbol{X}} = \boldsymbol{A}_3\boldsymbol{X} + \boldsymbol{B}_3 \tag{5}$$

$$\begin{cases} \boldsymbol{A}_3 = \begin{bmatrix} 0 & 0 & -1/L_1 & 0 \\ 0 & 0 & -1/L_2 & 0 \\ 1/C & 1/C & 0 & -u/C \\ 0 & 0 & u/L_g & 0 \end{bmatrix} \\ \boldsymbol{B}_3 = \begin{bmatrix} V_1/L_1 & 0 & 0 & 0 \\ 0 & V_2/L_2 & 0 & 0 \\ 0 & 0 & 0 & 0 \\ 0 & 0 & 0 & -V_g/L_g \end{bmatrix} \end{cases} \tag{6}$$

III. Dynamic Modeling of Converter

A. Averaged State Space MIMO Model

In the hybrid converter, duty cycles (d_1, d_2) of the boost

choppers and the amplitude modulation index u of the single-phase grid-connected inverter are assumed as controller inputs. Considering the averaging technique in Fig. 4, the general MIMO model of the system can be developed in all switching intervals of Fig. 3. The model includes all of the system control inputs as well as all of the state variables on both AC and DC sides.

$$\dot{\boldsymbol{X}} = \boldsymbol{A}_{\text{av}}\boldsymbol{X} + \boldsymbol{B}_{\text{av}} \tag{7}$$

where $\boldsymbol{A}_{\text{av}}$ and $\boldsymbol{B}_{\text{av}}$ are the averaged matrices, which can be calculated according to the durations of the switching intervals in Fig. 4 as:

$$\boldsymbol{A}_{\text{av}} = d_1\boldsymbol{A}_1 + (d_2 - d_1)\boldsymbol{A}_2 + (1 - d_2)\boldsymbol{A}_3 \tag{8}$$

$$\boldsymbol{B}_{\text{av}} = d_1\boldsymbol{B}_1 + (d_2 - d_1)\boldsymbol{B}_2 + (1 - d_2)\boldsymbol{B}_3 \tag{9}$$

By substituting (2), (4), and (6) into (8) and (9), the averaged state space [1] MIMO model of the system can be obtained as:

$$\begin{bmatrix}\dot{x}_1\\ \dot{x}_2\\ \dot{x}_3\\ \dot{x}_4\end{bmatrix} = \begin{bmatrix} 0 & 0 & \dfrac{d_1-1}{L_1} & 0 \\ 0 & 0 & \dfrac{d_2-1}{L_2} & 0 \\ \dfrac{1-d_1}{C} & \dfrac{1-d_2}{C} & 0 & -\dfrac{u}{C} \\ 0 & 0 & \dfrac{u}{L_g} & 0 \end{bmatrix}\begin{bmatrix}x_1\\ x_2\\ x_3\\ x_4\end{bmatrix} + \begin{bmatrix} \dfrac{V_1}{L_1} & 0 & 0 & 0 \\ 0 & \dfrac{V_2}{L_2} & 0 & 0 \\ 0 & 0 & 0 & 0 \\ 0 & 0 & 0 & -\dfrac{V_g}{L_g} \end{bmatrix} \tag{10}$$

B. Model Linearization

Considering small-signal linearization theory, state variables, duty cycles, and amplitude modulation, the index of the model can be assumed as:

$$\begin{cases} x_i = \bar{X}_i + \tilde{x}_i & i = 1,2,3,4 \\ d_j = \bar{D}_j + \tilde{d}_j & j = 1,2 \\ u = \bar{U} + \tilde{u} \end{cases} \tag{11}$$

where DC components $(\bar{X}_i, \bar{D}_j, \bar{U})$ are the nominal values of the parameters in an operation point of the converter; and AC components $(\tilde{x}_i, \tilde{d}_j, \tilde{u})$ are the small signal perturbations of the parameters around an operation point.

By substituting (11) into (10), the linearized small-signal model of the converter can be obtained. It should be noted that in the linearized model, the higher-order terms where two AC components are multiplied, are neglected.

$$\begin{cases} \dot{\tilde{\boldsymbol{x}}} = \boldsymbol{A}\tilde{\boldsymbol{x}} + \boldsymbol{B}\tilde{\boldsymbol{v}} \\ \tilde{\boldsymbol{y}} = \boldsymbol{C}\tilde{\boldsymbol{x}} \end{cases} \tag{12}$$

where $\tilde{\boldsymbol{x}}$, $\tilde{\boldsymbol{v}}$, and $\tilde{\boldsymbol{y}}$ are the state variable vector, control vector, and output vector of the system, respectively. Matrices of the linearized state space model can be rewritten as:

$$\begin{cases} \boldsymbol{A} = \begin{bmatrix} 0 & 0 & (\bar{D}_1 - 1)/L_1 & 0 \\ 0 & 0 & (\bar{D}_2 - 1)/L_2 & 0 \\ (1-\bar{D}_1)/C & (1-\bar{D}_2)/C & 0 & -\bar{U}/C \\ 0 & 0 & \bar{U}/L_g & 0 \end{bmatrix} \\ \boldsymbol{B} = \begin{bmatrix} \bar{X}_3/L_1 & 0 & 0 \\ 0 & \bar{X}_3/L_2 & 0 \\ -\bar{X}_1/C & -\bar{X}_2/C & -\bar{X}_4/C \\ 0 & 0 & \bar{X}_3/L_g \end{bmatrix} \\ \boldsymbol{C} = \begin{bmatrix} 1 & 0 & 0 & 0 \\ 0 & 1 & 0 & 0 \\ 0 & 0 & 0 & 1 \end{bmatrix} \\ \tilde{\boldsymbol{x}} = [\tilde{i}_{L_1} \quad \tilde{i}_{L_2} \quad \tilde{v}_C \quad \tilde{i}_{L_g}] \\ \tilde{\boldsymbol{v}} = [\tilde{d}_1 \quad \tilde{d}_2 \quad \tilde{u}] \\ \tilde{\boldsymbol{y}} = [\tilde{i}_{L_1} \quad \tilde{i}_{L_2} \quad \tilde{i}_{L_g}] \end{cases} \tag{13}$$

where $\tilde{i}_{L_1}$, $\tilde{i}_{L_2}$, $\tilde{v}_C$, and $\tilde{i}_{L_g}$ are the small signal perturbations of the i_{L_1}, i_{L_2}, v_C, and i_{L_g} around an operation point, respectively.

IV. Controller Design

The block diagram of the proposed controller for a grid-connected PV/FC hybrid energy system is shown in Fig. 5, where SPWM stands for sinusoidal pulse width modulation. The duty cycles of the DC-DC converters and inverter amplitude modulation index are the control inputs of the system. Furthermore, the output power of the PV/FC sources and injected AC current are the control outputs.

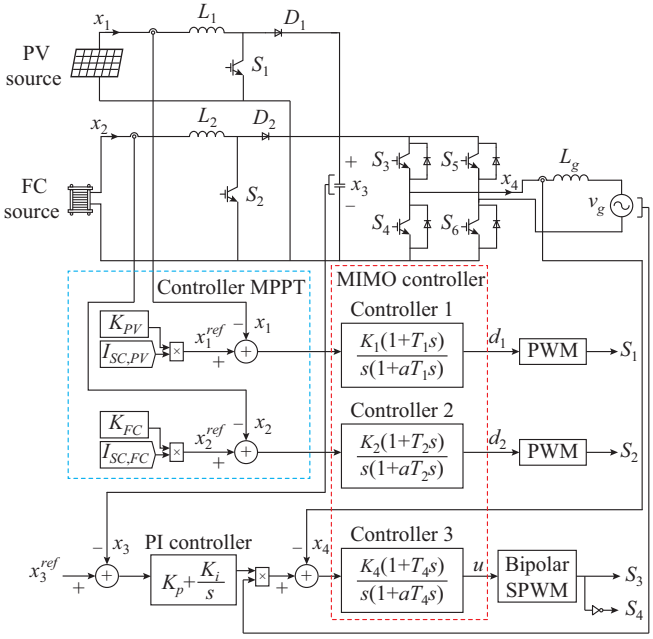

Fig. 5. Proposed control structure for grid-connected PV/FC hybrid energy system.

As shown in Fig. 5, the first control input d_1 is adjusted so that the operation of the PV source in MPP is established. To do this, at first, the reference value of the PV array current x_1^{ref}, which guarantees its operation in MPP, is calculated. Then, as shown in Fig. 5, the first controller determines d_1 according to the error of the first state variable ($e_1 = x_1^{ref} - x_1$). Similarly, d_2 is used for the MPPT of the FC power source. The values of the reference currents for PV and FC input power sources can be calculated according to the fractional short-circuit approach as $x_i^{ref} = K_{PV} I_{SC,PV}$ and $x_i^{ref} = K_{FC} I_{SC,FC}$, where $K_{PV} = 0.75$ and $K_{FC} = 0.85$ are the coefficients of the PV and FC reference currents, respectively; and $I_{SC,PV}$ and $I_{SC,FC}$ are the short-circuit currents of the PV and FC, respectively [26].

Alternatively, the amplitude modulation index of the inverter u is controlled to adjust the AC grid current on its reference value. It is obvious that the grid reference current must be selected so that all of the power generated by renewable input sources is injected into the power grid. To accomplish this, another separate controller is employed for the voltage control of the DC-link capacitor.

If the voltage of the DC-link capacitor is stabilized at a certain reference value x_3^{ref}, it can be concluded that all of the active power generated by DC sources is transferred into the power grid. In fact, if the power generated by renewable sources from one side and the injected AC power into the power grid from the other side are not equal, the power difference will be transferred into the DC-link capacitor and therefore, the voltage of the DC-link capacitor cannot be kept constant at its reference value. Briefly, the stabilization of the DC-link voltage at its reference value and the calculation of the power grid reference current based on the DC-link voltage error ensure that all of the power generated by renewable sources is transferred into the power grid.

As shown in Fig. 5, a cascade structure is proposed for closed-loop control of the grid-connected inverter. At first, according to the DC-link voltage error, the proportional-integral (PI) controller determines the amplitude of the grid reference current. Then, another controller is employed for regulation of the grid current. It is clear that for satisfactory control of the AC current controller, the DC-link reference voltage must be larger than the peak value of the grid voltage. It should be noted that in this study, the reference value of the DC-link capacitor is assumed to be 200 V.

Considering the Laplace transform of (12), the following equations can be obtained:

$$\tilde{\boldsymbol{y}} = \boldsymbol{G}\tilde{\boldsymbol{v}} \tag{14}$$

$$\boldsymbol{G} = \boldsymbol{C}(s\boldsymbol{I} - \boldsymbol{A})^{-1}\boldsymbol{B} \tag{15}$$

where $\boldsymbol{G}$ is the transfer function of the system; s is the operator variable in Laplace domain; and $\boldsymbol{I}$ is an identity matrix. Considering the inputs and outputs of the proposed MIMO system, (14) can be rewritten as follows:

$$\begin{bmatrix} y_1 \\ y_2 \\ y_3 \end{bmatrix} = \begin{bmatrix} \tilde{x}_1 \\ \tilde{x}_2 \\ \tilde{x}_4 \end{bmatrix} = \begin{bmatrix} g_{11} & g_{12} & g_{13} \\ g_{21} & g_{22} & g_{23} \\ g_{31} & g_{32} & g_{33} \end{bmatrix} \begin{bmatrix} \tilde{d}_1 \\ \tilde{d}_2 \\ \tilde{u} \end{bmatrix} \tag{16}$$

The simplified values of the transfer functions (g_{ij}, i, j = 1, 2, 3) are presented in the Supplementary Material.

From (16), it can be observed that all of the output variables of the system ($\tilde{x}_1$, $\tilde{x}_2$, and $\tilde{x}_4$) are related to all of the control inputs $\tilde{d}_1$, $\tilde{d}_2$, and $\tilde{u}$. Hence, it is not straightforward to design MPPT and AC current controllers. For this reason, a compensation network [27] is employed in this study to facilitate the design process of closed-loop controllers, as shown in Fig. 6.

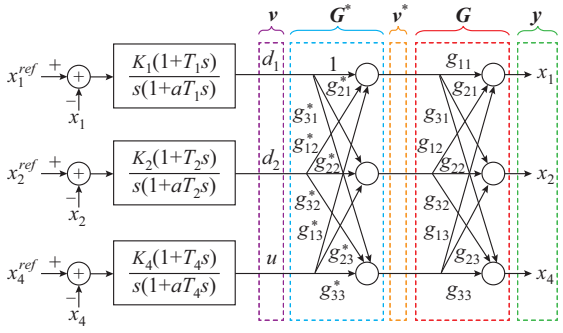

Fig. 6. Compensation network.

In fact, the compensation network is capable of decoupling multiple control loops of the proposed strategy. In the mentioned compensation network, the output vector $\boldsymbol{y}$ can be defined as $\boldsymbol{y} = \boldsymbol{G}\boldsymbol{v}^*$, where $\boldsymbol{v}^*$ is the modified control inputs, which can be defined as $\boldsymbol{v}^* = \boldsymbol{G}^*\boldsymbol{v}$. Therefore, it can be concluded that $\boldsymbol{y} = \boldsymbol{G}\boldsymbol{G}^*\boldsymbol{v}$. Thus, to decouple the control loops, the $\boldsymbol{G}\boldsymbol{G}^*$ must be a diagonal unity matrix. Then, each control output will only be related to the corresponding control input. With respect to these equations, it can be concluded that $\boldsymbol{G}^* = \boldsymbol{G}^{-1}\boldsymbol{x}\boldsymbol{v}^{-1}$, which is given in (17).

$$\boldsymbol{G}^* = \begin{bmatrix} 1 & \dfrac{g_{13}g_{32} - g_{12}g_{33}}{g_{11}g_{33} - g_{13}g_{31}} & \dfrac{g_{12}g_{23} - g_{13}g_{22}}{g_{11}g_{22} - g_{12}g_{21}} \\ \dfrac{g_{23}g_{31} - g_{21}g_{33}}{g_{22}g_{33} - g_{23}g_{32}} & 1 & \dfrac{g_{13}g_{21} - g_{11}g_{23}}{g_{11}g_{22} - g_{12}g_{21}} \\ \dfrac{g_{21}g_{32} - g_{22}g_{31}}{g_{22}g_{33} - g_{23}g_{32}} & \dfrac{g_{12}g_{31} - g_{11}g_{32}}{g_{11}g_{33} - g_{13}g_{31}} & 1 \end{bmatrix} \tag{17}$$

According to Fig. 6, by substituting $\boldsymbol{G}^*$ and $\boldsymbol{G}$ from (17) and (16) into $\boldsymbol{x} = \boldsymbol{G}\boldsymbol{G}^*\boldsymbol{v}$, the decoupled transfer functions of the system can be obtained as:

$$H_1(s) = \frac{\tilde{x}_1}{\tilde{d}_1} = g_{11} + g_{12}\frac{g_{23}g_{31} - g_{21}g_{33}}{g_{22}g_{33} - g_{23}g_{32}} + g_{13}\frac{g_{21}g_{32} - g_{22}g_{31}}{g_{11}g_{22} - g_{12}g_{21}} \tag{18}$$

$$H_2(s) = \frac{\tilde{x}_2}{\tilde{d}_2} = g_{21}\frac{g_{13}g_{32} - g_{12}g_{33}}{g_{11}g_{33} - g_{13}g_{31}} + g_{22} + g_{23}\frac{g_{12}g_{31} - g_{11}g_{32}}{g_{11}g_{33} - g_{13}g_{31}} \tag{19}$$

$$H_4(s) = \frac{\tilde{x}_4}{\tilde{u}} = g_{31}\frac{g_{12}g_{23} - g_{13}g_{22}}{g_{11}g_{22} - g_{12}g_{21}} + g_{32}\frac{g_{13}g_{21} - g_{11}g_{23}}{g_{11}g_{22} - g_{12}g_{21}} + g_{33} \tag{20}$$

Considering the developed transfer functions in (18)-(20), the proposed control loops in Fig. 6 can be designed. It should be noted that the control functions in the Laplace domain are assumed as $K_i(1 + T_i s)/[s(1 + aT_i s)]$, where $i = 1, 2, 4$. Therefore, it is possible to eliminate the steady-state error of

the system by considering integral terms in the compensators. These controllers are tuned to achieve a desirable phase margin in the range of [65°, 80°] with an acceptable cut-off frequency. The Bode plots of the controllers are illustrated in Fig. 7 before and after compensation according to the selected compensation gains in Table I.

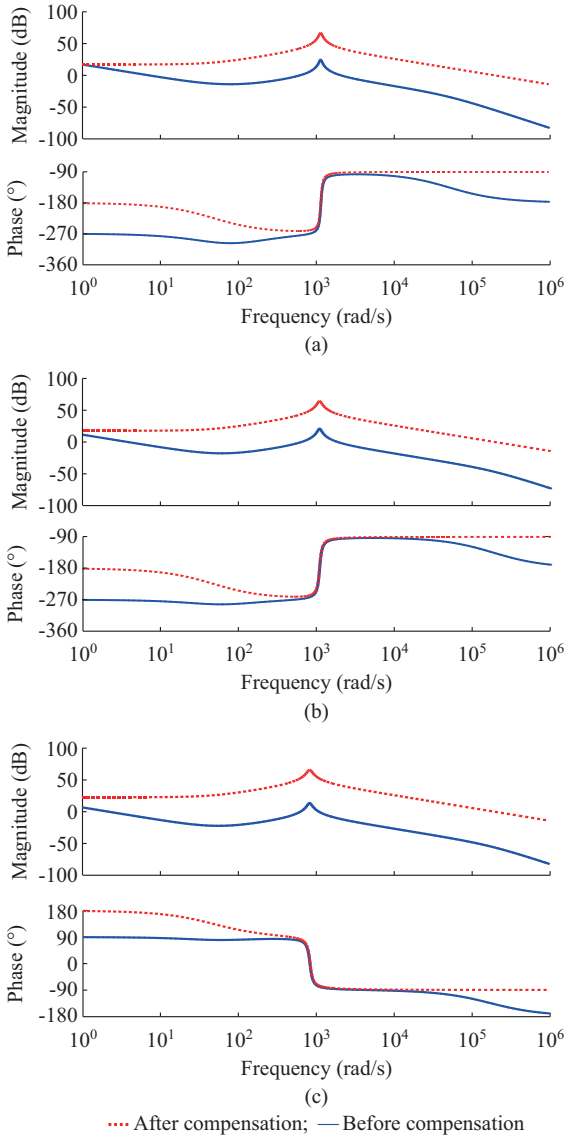

Fig. 7. Frequency response of closed-loop system before and after compensation. (a) Bode plot of $H_1(s)$ before and after compensation. (b) Bode plot of $H_2(s)$ before and after compensation. (c) Bode plot of $H_4(s)$ before and after compensation.

TABLE I
CONTROLLER GAINS

Controller	Gain		
	K_i	T_i	aT_i
Current controller of PV source $H_1(s)$	0.98550	0.007491	0.00001916
Current controller of FC source $H_2(s)$	0.32570	0.005260	0.00002005
AC current controller of power grid $H_4(s)$	0.15835	0.014893	0.00000562

V. SIMULATION RESULTS

To evaluate the accuracy of the proposed control method, simulation results of the designed hybrid energy system are presented in this section using the MATLAB/Simulink toolbox.

To model the BP585 PV input source in simulations using the electrical parameters of Table II, the equivalent circuit of Fig. 8 is employed. Nominal values of the system parameters are listed in Table III.

TABLE II
PV MODULE PARAMETERS

Parameter	Value
Number of cells N_s	36
Standard light intensity S_o	1000 W/m^2
Reference temperature T_{ref}	25 °C
Series resistance R_s	0.008 Ω
Short-circuit current I_{SC0}	5 A
Saturation current I_{S0}	3.8074×10^{-8} A
Band energy E_g	1.12 eV
Ideality factor A	1.2
Temperature coefficient C_t	0.00065 A/°C

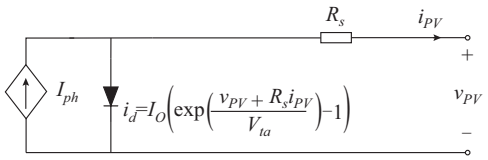

Fig. 8. Equivalent circuit of PV input source.

TABLE III
NOMINAL PARAMETERS OF POWER CIRCUIT

Simulation parameter	Value
Switching frequency of inverter and DC-DC converters f_s	20 kHz
PV inductor L_1	1 mH
FC inductor L_2	1 mH
Grid inductor L_g	1 mH
DC-link capacitor C	470 μF
Voltage of PV sources V_1	159.3 V
Voltage of FC sources V_2	150 V
AC grid frequency f	50 Hz
AC grid voltage V_g	110 V

Hence, current-voltage characteristics of the PV panel can be written as:

$$i_{PV}=I_{ph}-I_O\left(\exp\left(\frac{v_{PV}+R_s i_{PV}}{V_{ta}}\right)-1\right) \tag{21}$$

where i_{PV} and v_{PV} are the current and voltage of the PV panel, respectively; I_{ph} and I_O are the photo-generated and reverse saturation currents, respectively; R_s is the series resistance; and $V_{ta}=N_S A K_B T_{PV}/q$ is the thermal voltage, and A, K_B, q, and T_{PV} are the diode quality factor, Boltzmann constant, electron charge, and PV module temperature, respectively.

In addition, the photo-generated current I_{ph} depends on the

irradiance level and temperature as follows:

$$I_{ph} = I_{SC}\frac{S}{S_0} + C_t(T_a - T_0) \tag{22}$$

where I_{SC} is the short-circuit current of the panel; T_0 and S_0 are the nominal temperature and irradiance, respectively; S and T_a are the ambient irradiance and temperature, respectively; and C_t is the temperature coefficient.

Furthermore, as shown in Fig. 9, a controlled voltage source E with an internal resistance R can be considered for modeling the FC stack in nominal conditions. During the simulations, it is assumed that $E = 150$ V and $R = 0.2$ Ω.

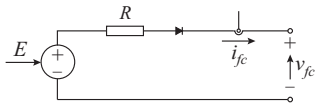

Fig. 9. Equivalent circuit of FC input source.

In Fig. 10, the simulation response of the proposed MIMO controller for the grid-connected PV/FC hybrid energy system in nominal condition is illustrated during steady-state operation.

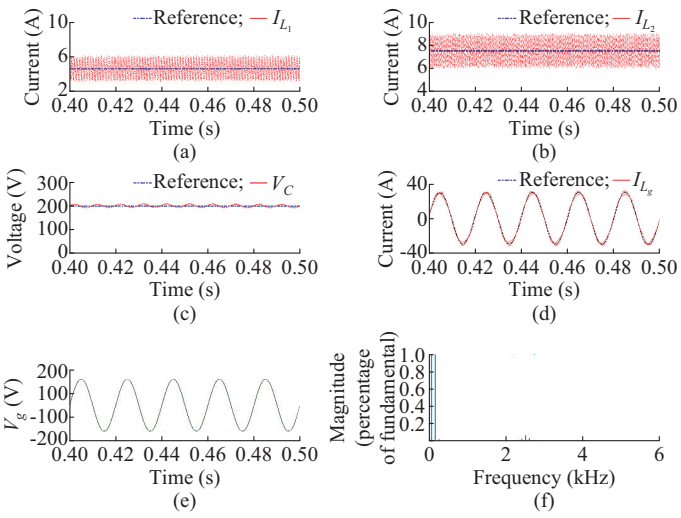

Fig. 10. Steady-state response of proposed MIMO controller for grid-connected PV/FC hybrid energy system. (a) Output current of PV source. (b) Output current of FC stack. (c) Voltage of DC-link capacitor. (d) Grid current versus its reference value. (e) Grid voltage. (f) Total harmonic distortion (THD) of grid current.

It is assumed that $T_a = 25$ °C and $S = 1000$ W/m^2. Hence, the reference current of the PV panel will be equal to 4.7 A in MPP. Moreover, the reference current of the FC stack is assumed to be 7.3 A. In Fig. 10(a) and (b), currents of the input renewable sources are illustrated versus references. It is shown that the proposed MIMO controller is able to stably regulate the DC-DC converters with zero steady-state error. Additionally, according to Fig. 10(c), voltage of the DC-link capacitor is regulated in its reference value. As a result, it can be concluded that all active power generated by the renewable source is injected into the grid. The grid reference current generated according to the DC-link voltage error is shown in Fig. 10(d). Considering Fig. 10(d) and (e), the AC current is injected in phase with voltage into the power grid with zero steady-state error. Moreover, the THD of the grid current is shown in Fig. 10(f), where when the fundamental (50 Hz) is equal to 22.55, THD equals 1.48%. The THD of the injected AC current is equal to 1.47%, which is completely compatible with the standards of a distribution network.

In Fig. 11, the transient response of the developed MIMO controller is illustrated during system start-up process. It is assumed that reference values of the input sources are changed from zero to nominal values. Furthermore, considering step changes of the reference voltage of DC-link capacitor from 0 to 200 V, the grid reference current is determined in the outer loop of the AC-side MIMO controller. It is observed that the proposed MIMO controller is stable and fast during system start-up process.

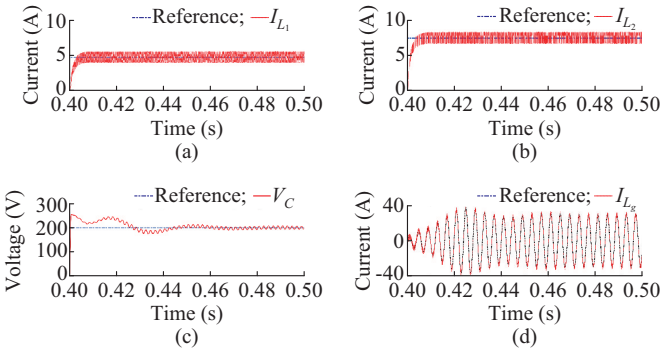

Fig. 11. Transient response of proposed MIMO controller during start-up process of grid-connected PV/FC hybrid energy system. (a) Transient response of PV panel. (b) Transient response of FC stack. (c) Transient response of DC-link capacitor voltage. (d) Grid current.

In Fig. 12, the transient response of the proposed MIMO controller during step changes of the PV reference current is illustrated. It is assumed that the radiation level is changed from 1000 to 600 W/m^2 at $t = 0.5$ s. Hence, the reference current of the PV panel is changed from 4.7 to 2.8 A. The proposed MIMO controller is able to regulate input current of the PV panel in MPP. Moreover, in spite of grid current changes, the DC-link voltage is stably regulated in its reference value.

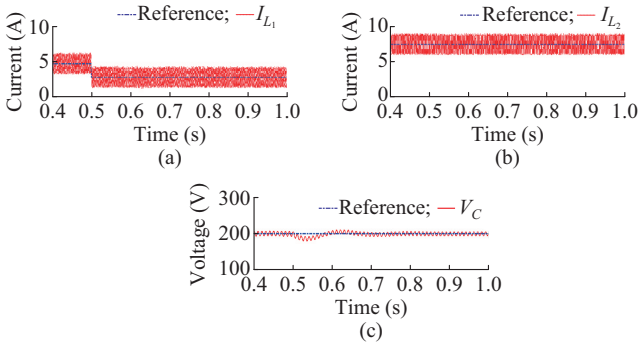

Fig. 12. Transient response of proposed MIMO controller during step changes of PV reference current. (a) Current of PV panel. (b) Current of FC stack. (c) DC-link capacitor voltage.

Similarly, in Fig. 13, the response of the proposed MIMO controller during step changes of the FC reference current is

illustrated. It is assumed that at $t=0.5$ s, the reference of the FC-side output current is stepped from 7.5 to 13 A. Finally, in Fig. 14, both of the DC reference currents are simultaneously changed. In fact, at $t=0.5$ s, the reference current of the PV panel and FC stack are changed from 4.7 to 2.8 A and from 7.5 to 13 A, respectively. It is clear that the developed MIMO controller is stable in different operation points and has fast transient response with zero steady-state error.

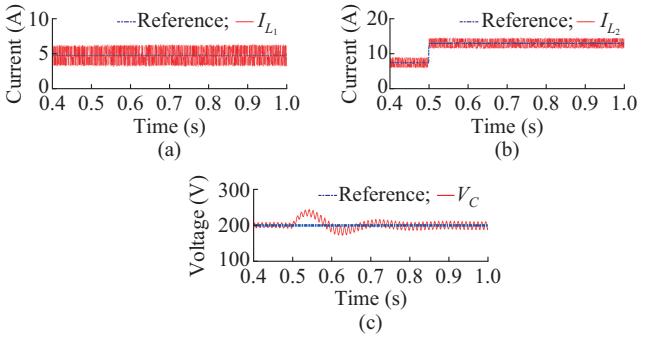

Fig. 13. Transient response of proposed MIMO controller during step changes of FC reference current. (a) Current of PV panel. (b) Current of FC stack. (c) DC-link voltage.

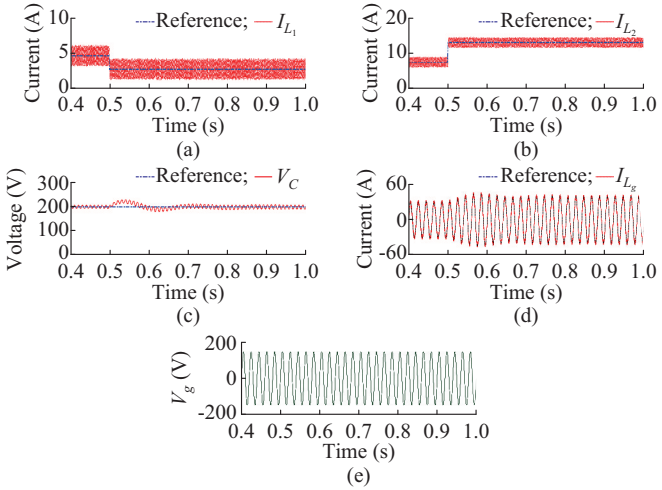

Fig. 14. Transient response of proposed MIMO controller during simultaneous step changes of PV and FC reference currents. (a) Current of PV panel. (b) Current of FC stack. (c) DC-link voltage. (d) Grid current. (e) Grid voltage.

In Fig. 15, the response of the designed MIMO controller to step changes of the DC-link reference voltage is shown. It is assumed that at $t=0.5$ s, the reference voltage of the DC-link capacitor is stepped from 200 to 250 V. It can be seen that the controller can track the changes of the reference value with a fast dynamic response and zero steady-state error.

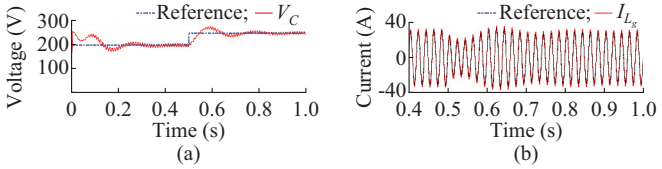

Fig. 15. Transient response of proposed MIMO controller during step changes of DC-link reference voltage. (a) Voltage of DC-link capacitor. (b) Grid current.

VI. Conclusion

In this study, a novel approach to design MIMO controller in grid-connected hybrid renewable energy systems is presented. The duty cycles of DC-DC converters and the amplitude modulation index of the grid-connected inverter are input variables of the MIMO controller. Additionally, control system outputs are defined as output current of the renewable sources and grid current. The developed MIMO closed-loop system is capable of MPPT for the PV/FC sources as well as the injection of generated power into the power grid. Considering the dependence of the control outputs on all of the control inputs, a special compensation network is developed to decouple the control loops. According to the frequency response of the system transfer functions, the control gains of the developed MIMO controller are tuned. The accuracy and effectiveness of the designed MIMO controller are evaluated by some simulations in the MATLAB/Simulink toolbox. According to the simulation results, the proposed MIMO controller is completely fast and stable at different operation points with zero steady-state error. Moreover, the THD of the grid current is approximately 1.48%, which is compatible with the standards of distribution networks.

References

[1] M. Salimi, J. Soltani, and A. Zakipour, "Experimental design of the adaptive backstepping control technique for single phase shunt active power filters," *IET Power Electronics*, vol. 10, no. 8, pp. 911-918, Jul. 2017.

[2] X. Chen, M. B. McElroy, Q. Wu *et al*., "Transition towards higher penetration of renewables: an overview of interlinked technical, environmental and socio-economic challenges," *Journal of Modern Power Systems and Clean Energy*, vol. 7, no. 1, pp. 1-8, Aug. 2018.

[3] A. Ajami and P. A. Shayan, "Soft switching method for multiport DC/DC converters applicable in grid connected clean energy sources," *IET Power Electronics*, vol. 8, no. 7, pp. 1246-1254, Jul. 2015.

[4] K. Y. Lo, Y. M. Chen, and Y. R. Chang, "Bidirectional single-stage grid-connected inverter for a battery energy storage system," *IEEE Industrial Electronics Society*, vol. 64, no. 6, pp. 4581-4590, Jun. 2017.

[5] Z. Chen, Y. Chen, J. M. Guerrero *et al*., "Generalized coupling resonance modeling, analysis, and active damping of multi-parallel inverters in microgrid operating in grid-connected mode," *Journal of Modern Power Systems and Clean Energy*, vol. 4, no. 1, pp. 63-75, Jan. 2016.

[6] J. L. Duarte, M. Hendrix, and M. G. Simoes, "Three-port bidirectional converter for hybrid FC systems," *IEEE Transactions on Power Electronics*, vol. 22, no. 2, pp. 480-487, Mar. 2007.

[7] F. Z. Amatoul, M. T. Lamchich, and A. Outzourhit, "Design control of DC/AC converter for a grid connected PV systems with maximum power tracking using MATLAB/Simulink," in *Proceedings of 2011 International Conference on Multimedia Computing and Systems*, Ouarzazate, Morocco, Apr. 2011, pp. 1-6.

[8] M. Shayestegan, "Overview of grid-connected two-stage transformerless inverter design," *Journal of Modern Power Systems and Clean Energy*, vol. 6, no. 4, pp. 642-655, Jan. 2018.

[9] M. Das and V. Agarwal, "Design and analysis of a high-efficiency DC-DC converter with soft switching capability for renewable energy applications requiring high voltage gain," *IEEE Transactions on Industrial Electronics*, vol. 63, no. 5, pp. 2936-2944, May 2016.

[10] M. Salimi and M. Pornadem, "A modular transformerless DC-DC step-up converter with very high voltage gain and adjustable switch stress," *European Power Electronics and Drives*, vol. 28, no. 2, pp. 75-88, Feb. 2018.

[11] H. E. Fadil, F. Giri, and J. M. Guerrero, "Grid-connected of photovoltaic module using nonlinear control," in *Proceedings of IEEE International Symposium on Power Electronics for Distributed Generation Systems*, Aalborg, Denmark, Jun. 2012, pp. 119-124.

[12] Y. Shi, R. Li, Y. Xue *et al*., "High-frequency-link based grid-tied PV system with small DC-link capacitor and low-frequency ripple-free

maximum power point tracking," *IEEE Transactions on Power Electronics*, vol. 31, no. 1, pp. 328-339, Jan. 2016.
[13] J. Hu, Y. Shan, Y. Xu *et al*., "A coordinated control of hybrid AC/DC micro-grids with PV-wind-battery under variable generation and load conditions," *International Journal of Electrical Power & Energy Systems*, vol. 104, pp. 583-592, Jan. 2019.
[14] A. Djafour, M. S. Aida, and B. Azoui, "Photovoltaic assisted fuel cell power systems," *Energy Procedia*, vol. 50, pp. 306-313, Jul. 2014.
[15] A. D. Martin, J. M. Cano, J. F. A. Silva *et al*., "Backstepping control of smart grid-connected distributed photovoltaic power supplies for telecom equipment," *IEEE Transactions on Energy Conversion*, vol. 30, no. 4, pp. 1496-1504, Dec. 2015.
[16] M. Salimi, J. Soltani, G. A. Markadeh *et al*., "Indirect output voltage regulation of DC-DC buck/boost converter operating in continuous and discontinuous conduction modes using adaptive backstepping approach," *IET Power Electronics*, vol. 6, no. 4, pp. 732-741, Apr. 2013.
[17] C. Peng, P. Xie, L. Pan *et al*., "Flexible robust optimization dispatch for hybrid wind/photovoltaic/hydro/thermal power system," *IEEE Transactions on Smart Grid*, vol. 7, no. 2, pp. 751-762, Mar. 2016.
[18] H. M. Al-Masri and M. Ehsani, "Feasibility investigation of a hybrid on-grid wind photovoltaic retrofitting system," *IEEE Transactions on Industry Applications*, vol. 52, no. 3, pp. 1979-1988, May-Jun. 2016.
[19] J. D. Dasika, B. Bahrani, M. Saeedifard *et al*., "Multivariable control of single-inductor dual-output buck converters," *IEEE Transactions on Power Electronics*, vol. 29, no. 4, pp. 2061-2070, Apr. 2014.
[20] X. Guo and J. M. Guerrero, "Abc-frame complex-coefficient filter and controller based current harmonic elimination strategy for three-phase grid connected inverter," *Journal of Modern Power Systems and Clean Energy*, vol. 4, no. 1, pp. 87-93, Jan. 2016.
[21] A. Merabet, L. Labib, A. M. Y. M. Ghias *et al*., "Robust feedback linearizing control with sliding mode compensation for a grid-connected photovoltaic inverter system under unbalanced grid voltages," *IEEE Journal of Photovoltaics*, vol. 7, no. 3, pp. 828-838, May 2017.
[22] A. Merabet, L. Labib, and A. M. Y. M. Ghias, "Robust model predictive control for photovoltaic inverter system with grid fault ride-through capability," *IEEE Transactions on Smart Grid*, vol. 9, no. 6, pp. 5699-5709, Nov. 2018.
[23] Y. Geng, K. Yang, Z. Lai *et al*., "A novel low voltage ride through control method for current source grid-connected photovoltaic inverters," *IEEE Access*, vol. 7, pp. 51735-51748, Apr. 2019.
[24] J. J. E. Slotine and W. Li, *Applied Nonlinear Control*. London: Prentice Hall Press, 1991.
[25] N. Mohan, T. M. Undeland, and W. P. Robbins, *Power Electronics: Converters, Applications and Design*. New York: John Wiley & Sons Press, 1995.
[26] H. A. Sher, A. F. Murtaza, K. E. Addoweesh *et al*., "A new sensorless hybrid MPPT algorithm based on fractional short-circuit current measurement and P&O MPPT," *IEEE Transactions on Sustainable Energy*, vol. 6, no. 5, pp. 1426-1434, Jul. 2015.
[27] Z. Qian, O. Abdel-Rahman, M. Pepper *et al*., "Analysis and design for paralleled three-port DC/DC converters with democratic current sharing control," in *Proceedings of 2009 IEEE Energy Conversion Congress and Exposition*, San Jose, USA, Sept. 2009, pp. 1375-1382.

Mahdi Salimi received the B.S. and M.S. degrees in electrical engineering from the K. N. Toosi University of Technology, Tehran, Iran, in 2000 and 2002, respectively, and the Ph.D. degree in power electronics from Science and Research Branch, Islamic Azad University, Tehran, Iran, in 2012. Since 2003, he has been with the Islamic Azad University, where he is presently working as an Assistant Professor in the Department of Electrical Engineering. His research interests include the closed-loop control of power electronics converters, high-gain DC-DC converter, grid-connected inverter and renewable energy.

Fereshteh Radmand received the B.Sc. degree in electrical power engineering from the Islamic Azad University of Ahar, Ahar, Iran, in 2013, and her M.Sc. degree in electrical power engineering from the University of Ahar, Ahar, Iran, in 2015, where she is presently working towards the Ph.D. degree in electrical engineering. Her current research interests include power electronic converter and control, and renewable energy system.

Mansour Hosseini-Firouz received the B.E. degree in electrical engineering from the Ardabil Branch, Islamic Azad University, Ardabil, Iran, in 2003, the M.S. and Ph.D. degrees in electrical engineering from the Science and Research Branch, Islamic Azad University, Tehran, Iran, in 2005 and 2013, respectively. He is currently an Assistance Professor at the Ardabil Branch, Islamic Azad University. His research interests include power system, power electronics, reliability and electricity market.